Pet.Sci.(2013)10:112-119
DOI 10.1007/s12182-013-0257-6

Influence of catalyst support structure on ethene/decene metathesis and coke formation over WO_3/SiO_2 catalyst

Zheng Min, Chen Sheng-Li*, Zhang Jun-Hui, Liu Yan, Sang Lei, You Ju and Wang Xiao-Dong

State Key Laboratory of Heavy Oil Processing, China University of Petroleum, Beijing 102249, China

Abstract: 8wt%WO_3/SiO_2 metathesis (disproportionation) catalysts with different pore structures were prepared by the incipient-wetness-impregnation method. The as-synthesized catalysts were characterized by N_2 adsorption-desorption, scanning electron microscopy (SEM), X-ray diffraction (XRD), UV-visible diffuse reflectance spectroscopy (DRS) and scanning transmission electron microscopy–high-angle annular dark field (STEM HAADF). The results of STEM HAADF showed that WO_3 species were not uniformly distributed on the SiO_2 support. The experimental results of 8wt%WO_3/SiO_2 performance in ethene/decene metathesis revealed that the catalytic effect of 8wt%WO_3/SiO_2 catalyst and coke formation over it were closely related to the support pore structure: The 8wt%WO_3/SiO_2 catalyst with a more complicated pore structure showed better catalytic performance but the coke deposition rate was also faster.

Key words: Metathesis, WO_3/SiO_2 catalysts, pore structure, coke formation

1 Introduction

The catalyst used for olefin metathesis is comprised of at least one transition metal such as tungsten, rhenium, molybdenum, ruthenium and osmium, and the technology of alkene metathesis to produce propene has been improved significantly in recent decades (Shell Oil Company, 1992a, 1993b). Most catalysts used for aliphatic olefins metathesis are rhenium, molybdenum or tungsten oxide loaded on a porous inorganic support (Mol, 2004; van Schalkwyk et al, 2003; Zhao et al, 2009). Among them, WO_3/SiO_2 catalyst has drawn a lot of attention because of its insensitivity to trace amount of poisons (Hua et al, 2011a; Spamer et al, 2003).

For tungsten-based catalysts, a lot of research, aimed at calcination time, moist atmosphere performance, preparation procedures, tungsten loadings and support porous structure, has been conducted for investigating their metathesis catalytic performance (Huang et al, 2007a; 2007b; Liu et al, 2009; Hu et al, 2006; Wang et al, 2003). It is known that coke formation over WO_3/SiO_2 catalysts is serious because of high metathesis temperature (350-500 °C) (Hua et al, 2011b). Moodley et al (2007) have studied coke formation over WO_3/SiO_2 catalyst in the metathesis of 1-octene and 1-heptene to longer chain internal alkenes and the results indicated that heavier internal alkene products coked more rapidly than 1-octene. By the use of energy-filtered transmission electron microscopy (EFTEM), they found that WO_3/SiO_2 catalyst was still active even at high coke level because the coke was mainly formed over the supports rather than the active tungsten species.

To further understand the coke formation over WO_3/SiO_2 catalysts, we characterized 8wt%WO_3/SiO_2 metathesis catalysts with different pore structures by XRD, UV-Vis DRS, SEM and scanning transmission electron microscopy–high-angle annular dark field (STEM HAADF), and their catalytic performance in ethene/decene metathesis was evaluated, then the coking behavior of the catalyst was investigated.

2 Experimental

2.1 Catalyst preparation

Commercial silica gel (CSG) were provided by Qingdao Haiyang Co. Ltd, China, and a support (denoted as S40) was prepared by evaporation-driven self-assembly of 40 nm monodisperse SiO_2 spheres in our work. The two SiO_2 supports were separately impregnated with ammonium metatungstate solution, dried at 50 °C for 6 h, then at 100 °C for 2 h, finally calcined in a muffle. The temperature of the muffle was raised to 550 °C at 3 °C/min and kept for 5 h. The 8wt%WO_3/SiO_2 catalysts were thus obtained.

*Corresponding author. email: slchen@cup.edu.cn
Received September 7, 2011

2.2 Catalyst characterization

Adsorption isotherms of nitrogen at -196 °C were recorded on an automated surface area & pore size analyzer QUADRASORB-SI (Quantachrome Corporation, USA).

X-ray powder diffraction (XRD) data was obtained using a Diffraktometer D8 (Bruker AXS, Germany) using CuKa radiation in the 2θ range of 5°–50° with a scanning rate of 1 °/min.

UV-Vis DRS spectra was recorded on a UV-410 spectrophotometer (Hitachi, Janpan) with integrating sphere diffuse reflectance attachment.

The coke content was measured using a HIR-944B high-frequency infrared carbon & sulfur analyzer (Wuxi High-Speed Analysis Instrument Co., Ltd, China).

Scanning electron microscopy (SEM) analysis was performed using a field emission scanning electron microscope Quanta 200F (FEI Corporation, USA) with an accelerating voltage of 30 kV.

Transmission electron microscopy (TEM) analysis was conducted on a Tecnai G2 F20 field emission transmission electron microscope (FEI Corporation, USA) with an accelerating voltage of 200 kV. The sample powder was dispersed ultrasonically in ethanol for 15 min, then one drop of the suspension was added to a copper grid. After evaporation of C_2H_5OH, the samples were used for TEM analysis.

2.3 Evaluation of catalytic performance

The metathesis reactions were carried out in a down-flow fixed-bed stainless steel reactor (9mmΦ×400mm). The catalyst was pretreated in situ in a H_2/N_2 mixture (with a H_2/N_2 molar ratio of 10/90 and total flow rate of 40 mL/min) at 420 °C for 0.5 h, then treated in N_2 flow at 550 °C for 1 h, subsequently, the catalyst was cooled down to the metathesis temperature in flowing N_2. The metathesis reaction conditions are as follows: Temperature=400 °C, pressure=2.0 MPa, ethene : decene (mol) =10:1, SAHSV=0.76 mmol/(h·m^2) (SAHSV: Surface Area Hourly Space Velocity). SAHSV is calculated as follows:

$$SAHSV = \frac{n_{C_2^=} + n_{C_{10}^=}}{S \times m} \quad (1)$$

where $n_{C_2^=}$ is the flow rate of ethene, mmol/h; $n_{C_{10}^=}$ is the flow rate of decene, mmol/h; S is the specific surface area of supports, m^2/g; m is the mass of catalyst, g.

All the metathesis reaction products were analyzed using a gas chromatograph equipped with a flame ionization detector (FID) and a 50 m PONA capillary column (PONA is an acronym for Paraffins, Olefins, Naphthenes and Aromatics).

3 Results and discussion

3.1 Catalyst characterization

Fig.1 shows the SEM images of the S40 and CSG supports. It can be seen that the both SiO_2 supports were disordered accumulations of SiO_2 particles, but the particle size distribution of the S40 support was more uniform than that of the CSG. Table 1 and Fig. 2 show that the specific surface area and total pore volume of the CSG support were more than threefold higher that of the S40 support, and the pore diameter distribution of the CSG is broader than that of the S40, but the difference of their average pore diameter was not significant. Because the S40 was consisted of 40 nm monodisperse SiO_2 microspheres, its surface area was contributed by the outer surface area of the monodisperse SiO_2 microspheres, its pore size was controlled by the their diameter, and its pore volume was the voids of the their packing. It was noteworthy that the pore volume of the S40 was very small, indicating that monodisperse SiO_2 microspheres were closely packed. The BET specific surface area and pore volume of the CSG were much larger than those of S40, implying that the CSG had a bridge-structure and was comprised of nano-particles with internalr pores.

Table 1 Characterization results of structure properties of the supports

Structure properties	CSG	S40
Surface area BET, m^2·g^{-1}	416	113
Total pore volume, cm^3·g^{-1}	0.926	0.292
Average pore diameter, nm	8.91	10.31

The XRD patterns of supports and catalysts are shown in Fig. 3. It can be seen that no characteristic peaks of WO_3 crystallites (2θ: 23.12°, 23.60°, and 24.38°) were observed for pure CSG and S40 support. But the characteristic peaks of WO_3 crystallites were observed on the XRD patterns of catalysts 2θ 8wt%WO_3/CSG and 8wt%WO_3/S40 and their intensities were different, indicating that with the same WO_3 loading amount (by weight), these two 8wt%WO_3/SiO_2 catalysts had different densities of WO_3 crystallite on their surface because of the different specific surface areas of their supports. The surface concentration of WO_3 species can be calculated quantitatively as follows:

$$C_{WO_3} = \frac{m_{WO_3}/M_{WO_3}}{100 - m_{WO_3}} \times \frac{1}{S_{SiO_2}} \times N_A \times 10^{-18} \quad (2)$$

where C_{wo_3} is the WO_3 surface concentration on catalysts ($W^{6+}_{cations}/nm^2$); m_{wo_3} is the WO_3 loading amount (by weight); M_{wo_3} is the molecular weight of WO_3 (231.85, g·mol^{-1}); S_{sio_2} is the specific surface area of supports (m^2·g^{-1}); and N_A is the Avogadro constant (6.022×10^{23}, mol^{-1}).

Liu et al (1987) reported that the monolayer dispersion capacity of WO_3 on the surface of SiO_2 support was $0.46W^{6+}_{cations}/nm^2$ and WO_3 crystallites would be formed when the WO_3 loading exceeded this value. From Eq. (2), the WO_3 surface concentration was $0.543W^{6+}_{cations}/nm^2$ for 8wt%WO_3/CSG, which was 1.18 layers loading, slightly higher than a monolayer loading; and the WO_3 surface concentration was $1.986W^{6+}_{cations}/nm^2$ for 8wt%WO_3/S40, which was 4.32 layers loading, much greater than the monolayer loading. Thus, the size and amount of WO_3 crystallites formed on 8wt%WO_3/S40 would be greater than that on 8wt%WO_3/CSG, and the intensity of characteristic peaks (XRD) of 8wt%WO_3/S40

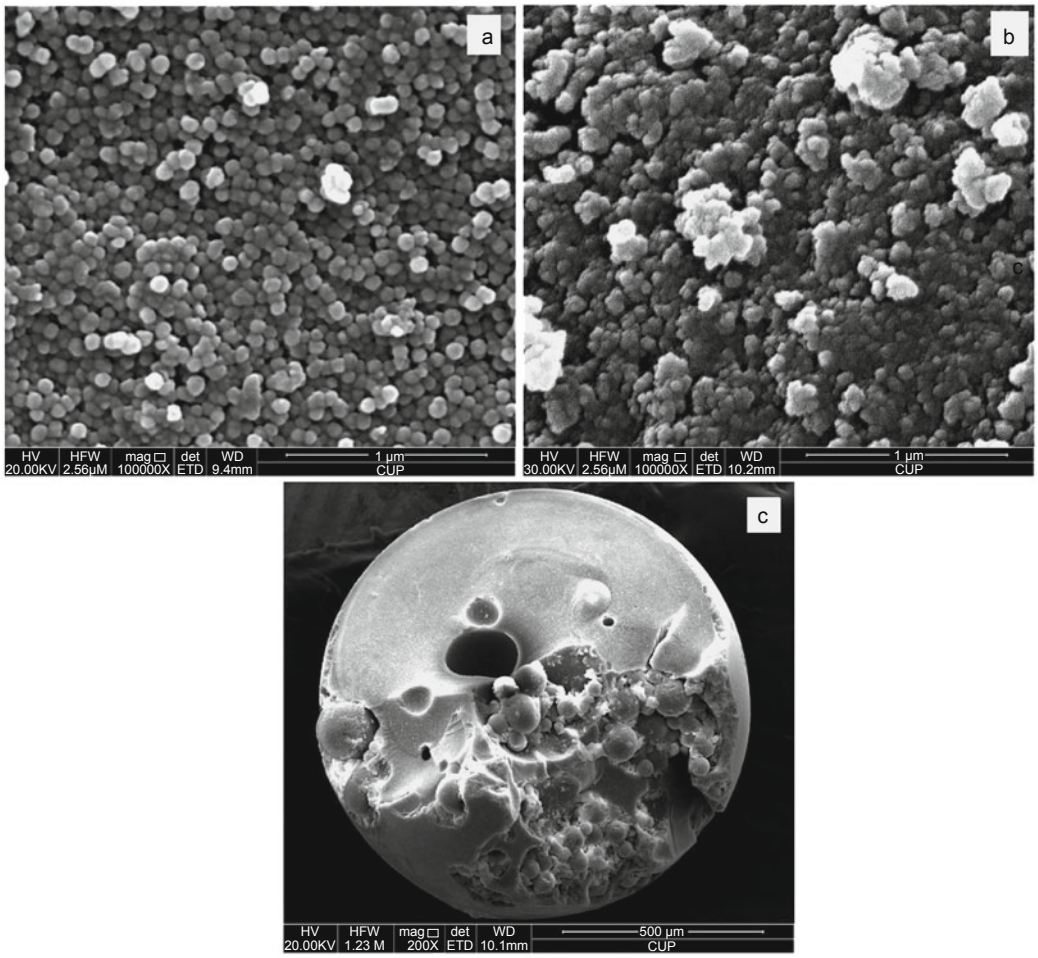

Fig. 1 SEM images of SiO_2 supports
a: the fracture surface of S40 support; b and c: the fracture surface of spherical CSG support

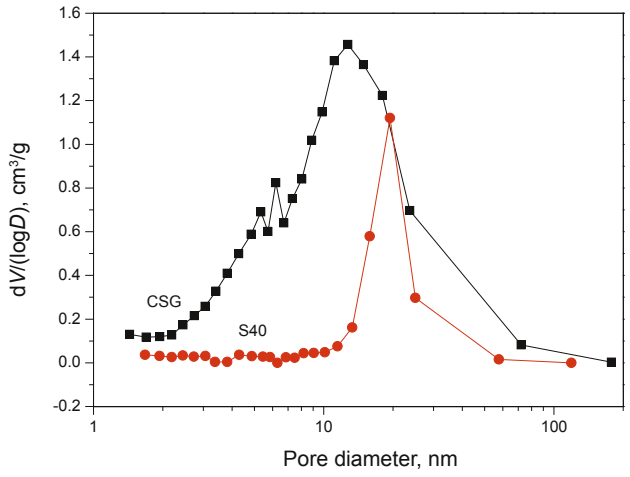

Fig. 2 Pore size distribution of supports

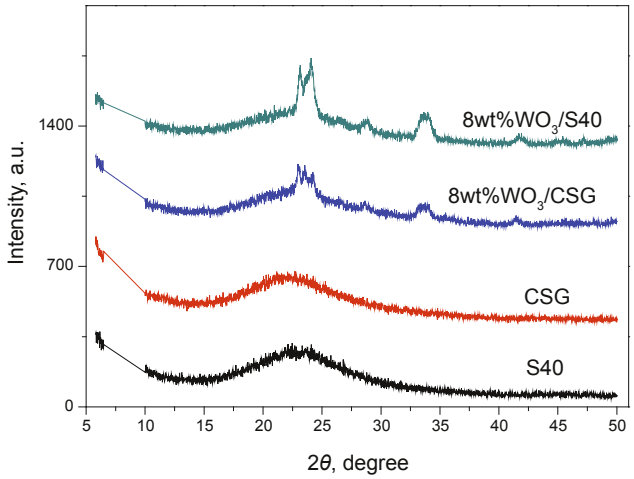

Fig. 3 Powder XRD patterns of different samples

would be stronger than that of 8wt%WO_3/CSG as shown in Fig. 3.

UV-Vis DRS spectra is a good way to investigate the coordination state of tungsten species over supports. The UV-Vis DRS spectra of different catalysts used in this work are shown in Fig. 4. It can be seen that the absorption bands of the fresh samples were observed in the region of 230-400 nm, with two subbands at 230 nm and 280-320 nm, respectively. The absorption bands of spent samples were observed in the region of 400-800 nm. According to the literature (Zhao et al, 2009), these subbands can be assigned as follows: The 230 nm band corresponds to tetrahedral W^{6+} species; The 280-320 nm band corresponds to octahedral polytungstate species; the 375-400 nm band corresponds to WO_3 crystallites, and the

400-800 nm bands correspond to W^{4+} and W^{5+} species. From Fig. 4, there were only tetrahedral W^{6+} species and octahedral polytungstate species on fresh catalysts. After pretreatment in a reducing atmosphere, W^{6+} species were reduced to W^{4+} and W^{5+} species which are the active species for metathesis reactions. Fig. 4 also shows that the absorption curves of sample (c) and sample (e) are similar to each other, suggesting that the valence state of tungsten species was unchanged in the metathesis reaction.

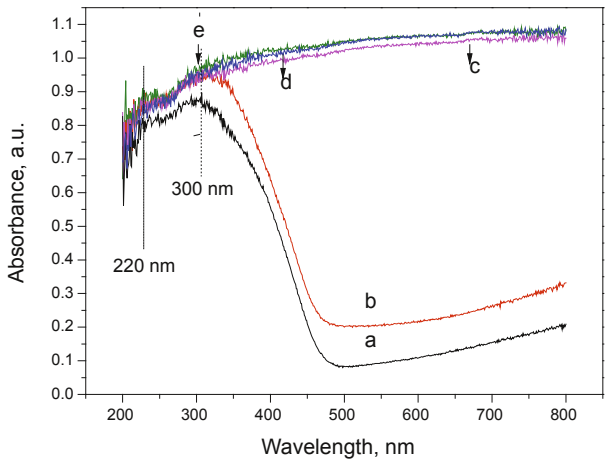

Fig. 4 UV-Vis DRS spectra of different samples
a: fresh 8wt%WO_3/S40; b: fresh 8wt%WO_3/CSG; c: spent 8wt%WO_3/CSG with 72 h online; d: spent 8wt%WO_3/S40 with 72 h online; e: spent 8wt%WO_3/CSG with 8 h online

Fig. 5 shows the SEM images of catalyst 8wt%WO_3/SiO_2 with different supports. Compared with Fig. 1, it can be seen that there is no significant difference in surface morphology between the 8wt%WO_3/SiO_2 catalysts and their corresponding suppots.

The images of TEM and STEM HAADF of catalysts are shown in Fig. 6. The TEM image (Fig. 6a) showed that the sphericity of 40 nm SiO_2 microspheres was not good, and the STEM HAADF images (Fig. 6b) and (Fig. 6c) show that WO_3 crystal particles of different sizes were formed. The STEM HAADF images (Fig. 6c) show that WO_3 crystallites form more easily at the junctions between SiO_2 microspheres, indicating that WO_3 species were not uniformly distributed on the S40 support. The TEM images (Fig. 6e) and STEM HAADF images (Fig. 6d, 6f), showed that the pore structure of CSG support was completely disordered. However, by comparing the images of the both catalysts in Fig. 6, it can be found that distribution of WO_3 species was more uniform on the CSG support than on the S40 support. This is because that

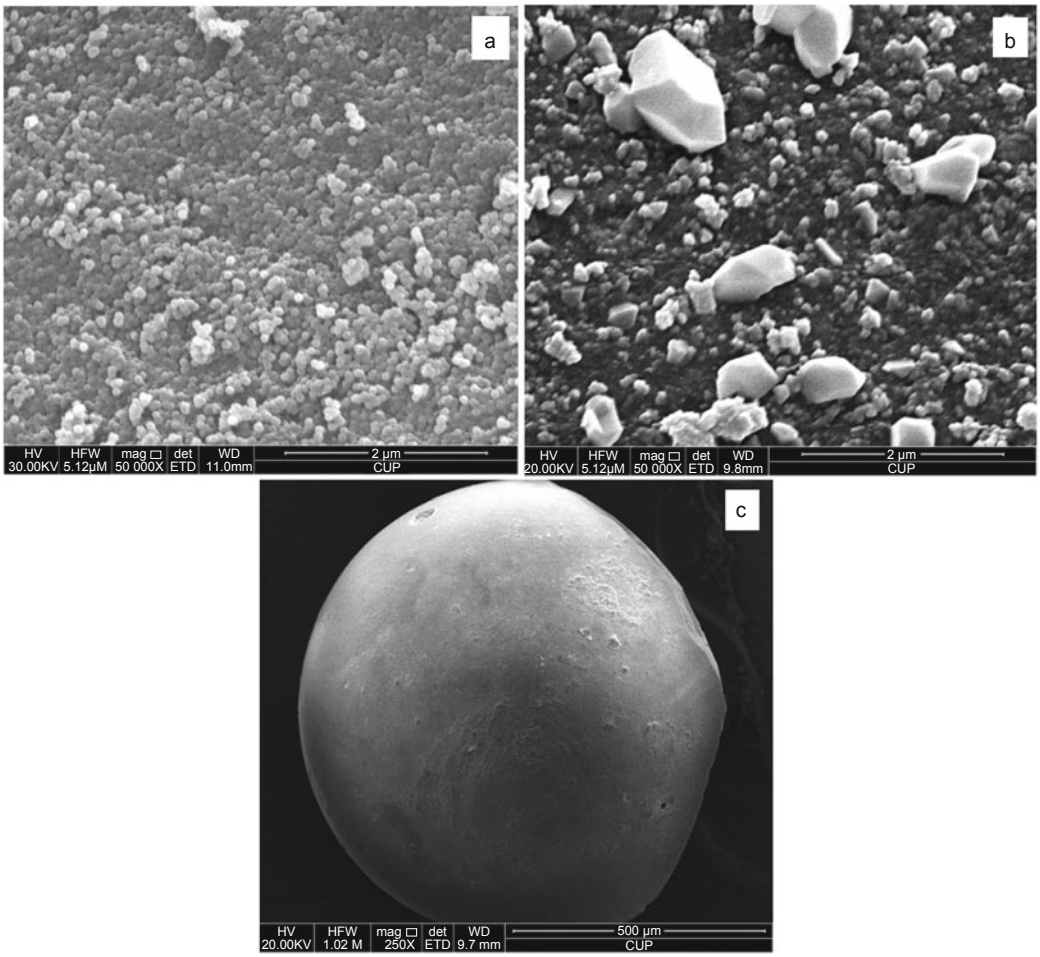

Fig. 5 SEM images of 8wt%WO_3/SiO_2 catalysts
a: the fracture surface of 8wt%WO_3/S40; b: the fracture surface of 8wt%WO_3/CSG; c: the external surface of spherical 8wt%WO_3/CSG

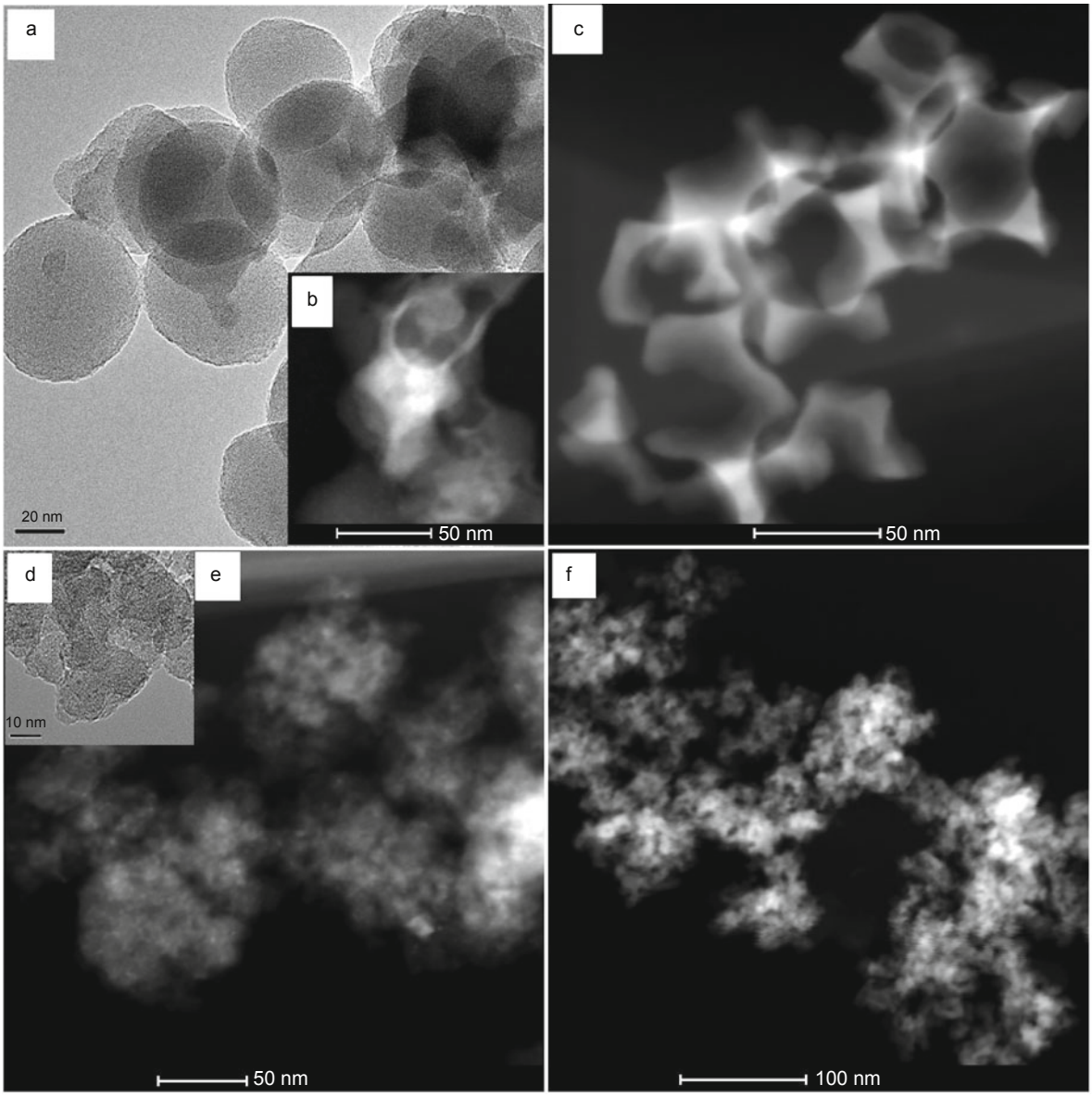

Fig. 6 STEM HAADF and TEM images of catalysts
a: bright field TEM of 8wt%WO_3/S40; b: STEM HAADF of 8wt%WO_3/S40; c: STEM HAADF of 8wt%WO_3/S40 after dissolving the SiO_2 support with HF; d: bright field TEM of 8wt%WO_3/CSG; e: STEM HAADF of 8wt%WO_3/CSG; f: STEM HAADF of 8wt%WO_3/CSG after dissolving the SiO_2 support with HF

the surface area of the S40 support is much smaller than that of the CSG support (Table 1), hence the surface concentration of WO_3 species on the surface of the CSG support was lower than that on the surface of the S40 support for the same WO_3 loading amount (in weight), as a result the particle size of WO_3 crystallite formed on S40 was bigger than that on CSG, the result is in accordance with that shown in Fig. 3.

3.2 Catalytic performance in ethylene/decene metathesis

According to the metal-carbene mechanism (Wilson et al, 1978), there are four reaction pathways in the ethene/decene metathesis system, namely self-metathesis, cross-metathesis, polymerization, and isomerization (double bond isomerization and skeleton isomerization), among which the cross-metathesis of ethene/decene is the main reaction. The possible product of ethene/decene metathesis is the olefins from ethene to 9-octadecylene, in which the 1-olefins from ethene to 1-decene are the products of ethene/decene cross-metathesis. Excessive ethene feedstock would promote further metathesis reaction of ethene with other products from C_4-C_9 olefins, and result in more products of short carbon (Shell Oil Company, 1992b, 1993a). Therefore selectivities of propene and C_6-C_9 were selected as the indicators of ethene/decene metathesis degree in this work.

Fig. 7 shows the effect of support properties on catalyst performance in the ethene/decene metathesis reaction. From Fig. 7, two interesting phenomena can be seen with catalyst 8wt%WO_3/S40: One is that an induction period existed for decene conversion, indicating that catalyst 8wt%WO_3/S40 was more difficult to activate than 8wt%WO_3/CSG; and the other is that the ethene conversion was negative after 27 h, indicating that the formation of ethene was greater than its consumption.

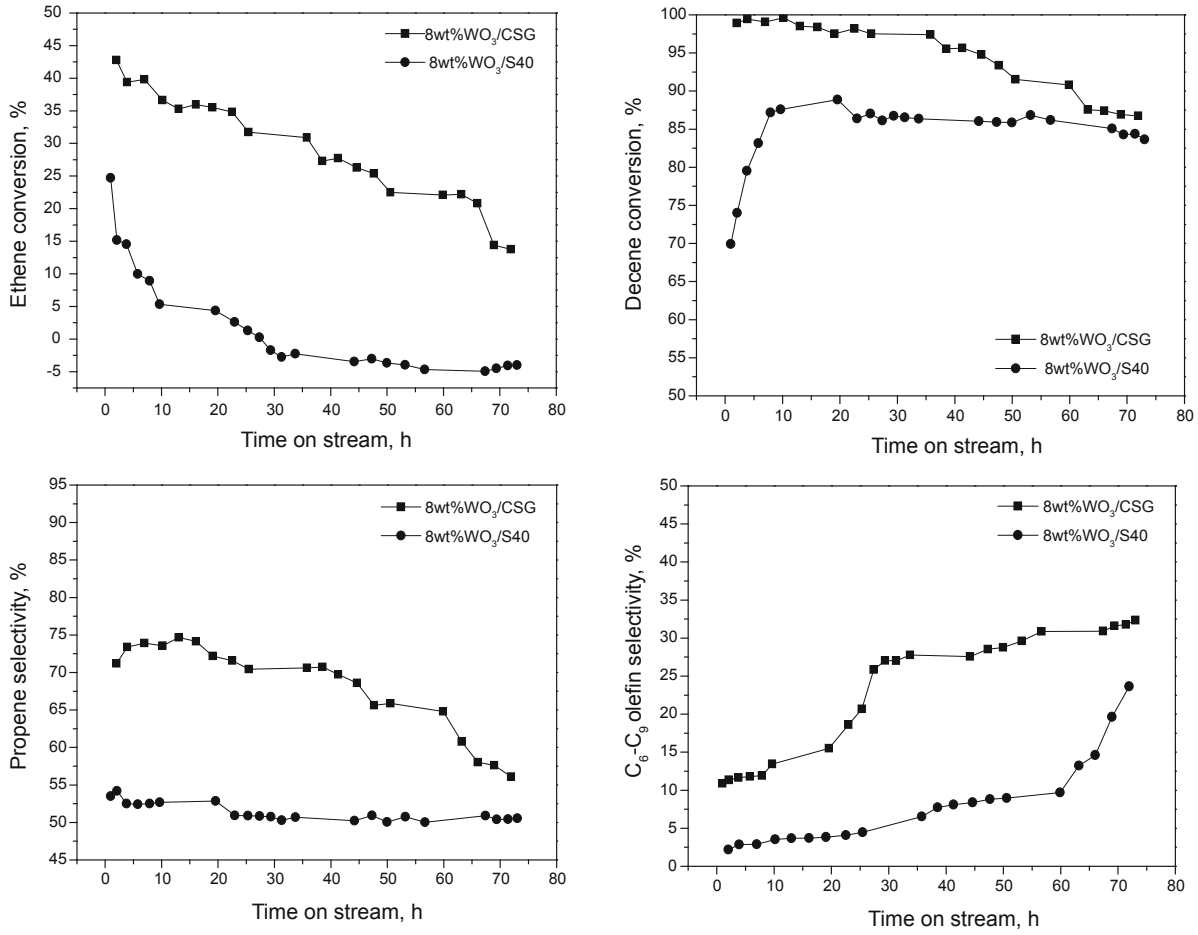

Fig. 7 Effect of support properties on catalyst performance in ethene/decene metathesis reaction (Reaction condition: P=2.0 MPa, T=400 °C, SAHSV=0.76 mmol/(h·m^2), C_2H_4:$C_{10}H_{20}$ (mol)=10:1)

The double bond isomerization of 1-olefins, an important reaction in the ethene/decene metathesis reaction system, would increase the yield of propene. For 8wt%WO_3/S40 catalyst, the S40 support had a simple pore structure (Table 1) compared with CSG support. At a certain point as the reaction proceeds, the double bond isomerization rate of 1-olefins might slow down, and then the possibility of cross-metathesis reactions between 1-olefins would increase. When the reaction rate between 1-olefins is fast enough, the formation of ethene would exceed its consumption (i.e. conversion), resulting in ethene conversion being negative, and correspondingly the C_3 selectivity would declined while C_6-C_9 selectivity would increased.

3.3 Coking during ethene/decene metathesis

The SEM images of spent catalyst are shown in Fig. 8. Compared with Fig. 1 and Fig. 5, it can be found that the superficial morphology of spent 8wt%WO_3/S40 catalyst was quite similar to that of S40 support and fresh 8wt%WO_3/S40 catalyst, and Fig. 8a reveals that the deposited coke over 8wt%WO_3/S40 coated the support surface. Flake-shaped coke deposits were clearly visible in the pores of spent catalyst 8wt%WO_3/CSG. This demonstrates that the morphology of coke deposits over the 8wt%WO_3/SiO_2 catalysts is different because of their different pore structures.

In the metathesis reaction, both feedstock and products are coke precursors, so coke formation over catalyst WO_3/SiO_2 during metathesis is a serious problem that cannot be ignored (Moodley et al, 2007). In the research onto coke formation, the Voorhies equation (Voorhies, 1945) is widely used because of its simplicity (Klemm et al, 2001; Gascón et al, 2003). Based on this equation, the relationship between the coke deposits on metathesis catalysts and the reaction time can be expressed as Eq. (3):

$$C_C = At^n \tag{3}$$

Usually, C_C is the weight of coke deposit per unit weight of catalyst (%) in literature, but in this work C_C is the surface concentration of coke deposit on the catalyst ($mg_{coke}/m^2_{catalyst}$), A and n are empirical constant in the modified Voorhies modeland, t (h or minute) is the reaction time.

Based on experimental data, the relationship of the amount of coke deposited with reaction time was fitted for catalysts 8wt%WO_3/CSG and 8wt%WO_3/S40 (see Fig. 9), and the values of A and n in Eq. (3) are obtained for the both catalysts. The classical Voorhies equation for 8wt%WO_3/CSG (Eq. 4) and 8wt%WO_3/S40 (Eq. 5) are as follows:

$$C_C = 0.00996 \times t^{0.9245} \tag{4}$$

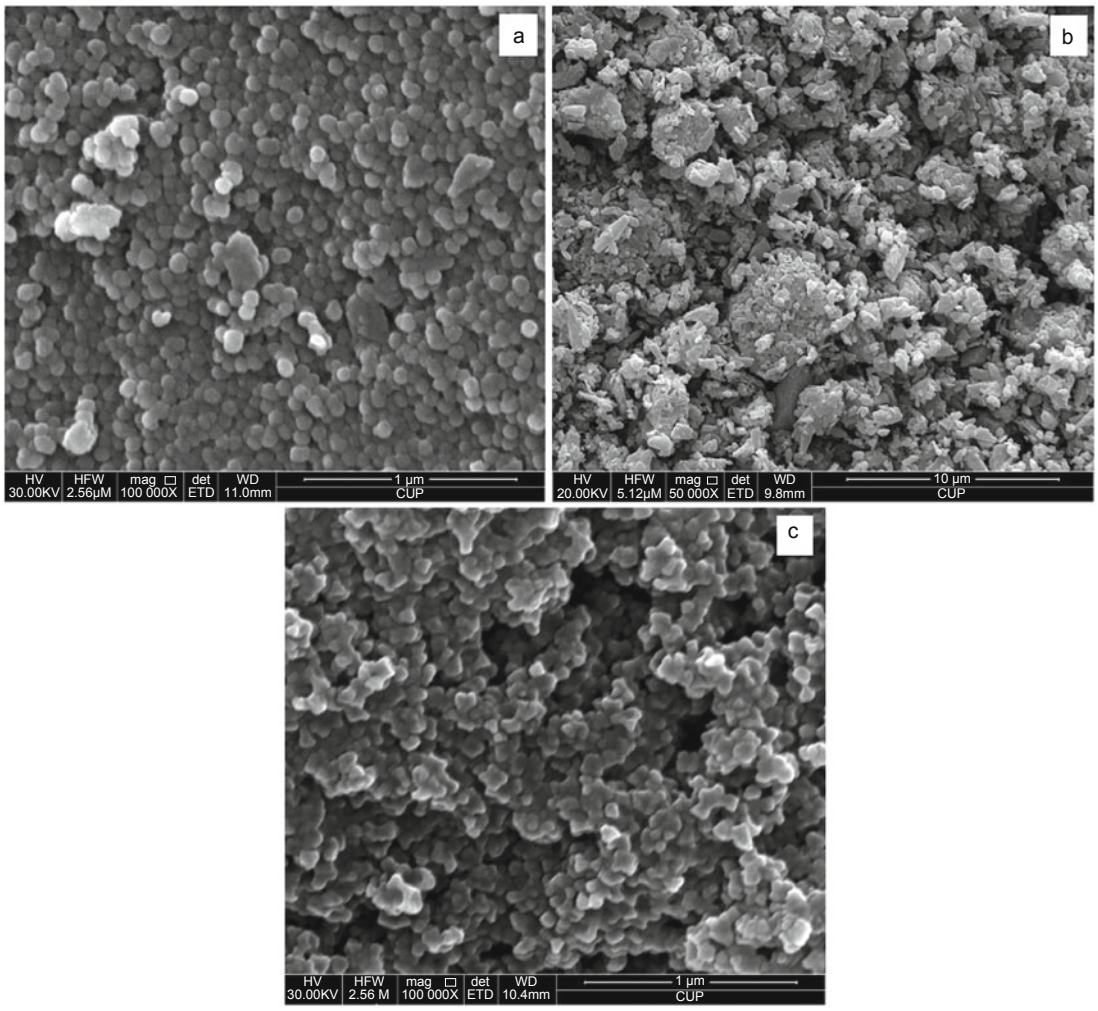

Fig. 8 SEM of spent catalysts and coke deposits
a: the fracture surface of spent 8wt%WO_3/S40 with an online time of 72 h; b: coke deposits over spent 8wt%WO_3/S40 catalyst after dissolving the SiO_2 support with HF; c: the fracture surface of spent 8wt%WO_3/CSG with an online time of 72 h

$$C_C = 0.0079 \times t^{0.8994} \quad (5)$$

Fig. 9 shows that the fitted curve agrees well with the experimental data. So the classical Voorhies equation can be used to quantitatively express the relationship between coke deposits on catalysts and reaction time. Eq. (4) and Eq. (5) showed that the coke formation was strongly influenced by the support structure of catalyst under the same reaction conditions.

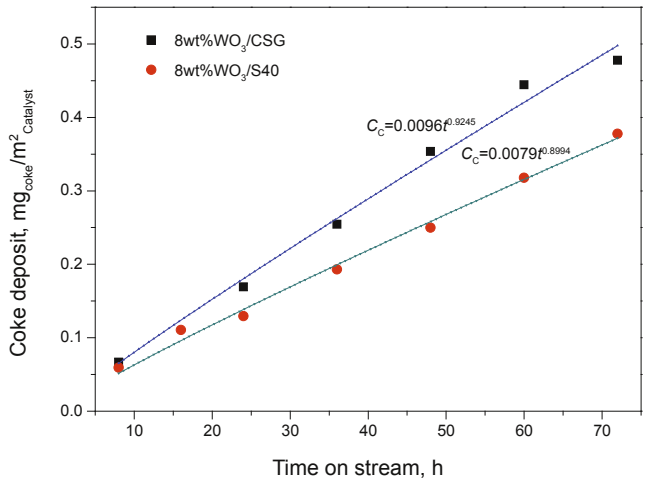

Fig. 9 Fitted curves and experimental data for coke deposited on catalyst with time

Substituting the values of A and n in Eq. (4) and Eq. (5) into the first-order derivative of Eq. (3), we obtain Eq. (6) and Eq. (7), which stand for the coke deposition rate as a function of reaction time for catalyst 8wt%WO_3/CSG (Eq. (6)) and 8wt%WO_3/S40 (Eq. (7)), respectively:

$$\frac{dC_C}{dt} = Ant^{(n-1)} = 0.0089t^{-0.0755} \quad (6)$$

$$\frac{dC_C}{dt} = Ant^{(n-1)} = 0.0071t^{-0.1006} \quad (7)$$

Substituting Eq. (3) and Eq. (4) into Eq. (6); and Eq. (3) and Eq. (5) into Eq. (7), we obtain Eq. (8) and Eq. (9), respectively, to describe the relationship between the deposited coke amount and the coke deposition rate over catalyst 8wt%WO_3/CSG (Eq. (8)) and 8wt%WO_3/S40 (Eq. (9)):

$$\frac{dC_C}{dt} = A^{\frac{1}{n}} n C_C^{\frac{n-1}{n}} = 0.0066 C_C^{-0.0755} \quad (8)$$

$$\frac{dC_C}{dt} = A^{\frac{1}{n}} n C_C^{\frac{n-1}{n}} = 0.0046 C_C^{-0.1118} \quad (9)$$

Fig. 10 shows the relationship between the coke deposition rate and reaction time. From Fig.10, for the both catalysts, it can be seen that the trend of their coke deposition rate was similar, namely the coke deposition rates both decreased with time, indicating that the acidity distribution on the both catalysts was not uniform (Mi et al, 2010). However, the coke deposition rate over catalyst 8wt%WO_3/CSG was greater than that over 8wt%WO_3/S40. Generally, coke was formed first at acid centers with high coking rate. However, the number of acid centers decreased with reaction time as they were covered by coke deposits and the coking rate decreased accordingly.

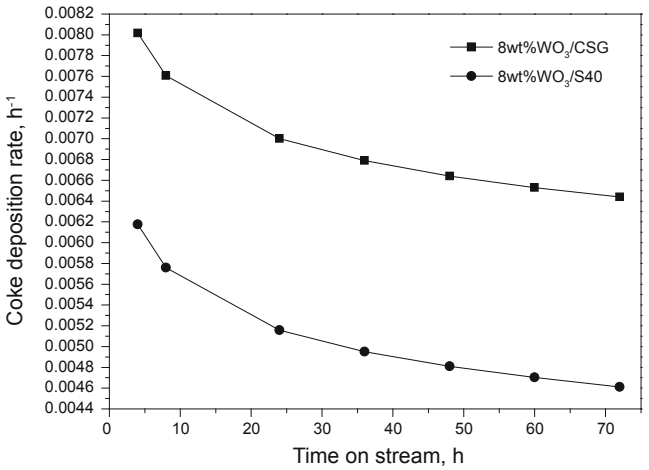

Fig. 10 The relationship between the coke deposition rate and reaction time

4 Conclusions

Two 8wt%WO_3/SiO_2 catalysts with different porous structures, namely, one support was commercial silica gel CSG with larger specific surface area, and the other was self-made S40 support with smaller specific surface area, were investigated and found that the WO_3 species surface concentration of 8wt%WO_3/CSG was close to the dispersion state of WO_3 monolayer loading because of its larger specific surface area. The WO_3 species were not uniformly distributed on the SiO_2 support, the higher the WO_3 surface concentration, the larger the crystalline size of WO_3. As a result, the 8wt%WO_3/CSG catalyst whose pore structure is more complicated showed better catalytic effect than that of 8wt%WO_3/S40 catalyst during the metathesis reaction in ethene/decene.

Coke deposition on WO_3/SiO_2 catalyst was also closely related to the pore structure of the support. The kinetic model of coke formation of ethene/decene metathesis can be expressed by the classical Voorhies equation, and the coking deposition rate on 8wt%WO_3/CSG catalyst is faster than that on 8wt%WO_3/S40 catalyst.

References

Gascón J, Téllez C, Herguido J, et al. Propane dehydrogenation over a Cr_2O_3/Al_2O_3 catalyst: Transient kinetic modeling of propene and coke formation. Appl. Catal. A. 2003. 248: 105-116

Hu J C, Wang Y D, Chen L F, et al. Synthesis and characterization of tungsten-substituted SBA-15: An enhanced catalyst for 1-butene metathesis. Micropor. Mesopor. Mat. 2006. 93: 158-163

Hua D, Chen S L, G M Yuan, et al. Metathesis of butene to propene on WO_3 supported on MTS-9 titanium-silica: Effect of loading on selectivity of product and yield of propene. Transition Met. Chem. 2011a. 36: 245-248

Hua D, Chen S L, Yuan G M, et al. Metathesis of butene to propene and pentene over WO_3/MTS-9. Micropor. Mesopor. Mat. 2011b. 36: 245-248

Huang S J, Chen F C, Liu S L, et al. The influence of preparation procedures and tungsten loading on the metathesis activity of ethene and 2-butene over supported WO_3 catalysts. J. Mol. Catal. Chem. 2007a. 267: 224-233

Huang S J, Liu S L, Zhu Q J, et al. The effect of calcination time on the activity of WO_3/Al_2O_3/HY catalysts for the metathesis reaction between ethene and 2-butene. Appl. Catal. A. 2007b. 323: 94-103

Klemm E, Amon B, Redlingshofer H, et al. Deactivation kinetics in the hydrogenation of nitrobenzene to anilineon the basis of a coke formation kinetics investigations in an isothermal catalytic wall reactor. Chem. Eng. Sci. 2001. 56: 1347-1353

Liu H J, Huang S J, Zhang L. The preparation of active WO_3 catalysts for metathesis between ethene and 2-butene under moist atmosphere. Catal. Commun. 2009. 10: 544-548

LiuY J, Wu J P, Guo Q L, et al. XRD and XPS studies of WO_3 on silica. Chin. J. Catal. 1987. 8(1): 14-18 (in Chinese)

Mi G, Li J, Qiu D, et al. Kinetics of coke formation on a Fe-ZSM-5 zeolite catalyst in the one-step oxidation of benzene to phenol with N_2O. Chin. J. Catal. 2010. 31: 547-551 (in Chinese)

Mol J C. Industrial applications of olefin metathesis. J. Mol. Catal. Chem. 2004. 213: 39-45

Moodley D J, van Schalkwyk C, Spamer A, et al. Coke formation on WO_3/SiO_2 metathesis catalysts. Appl. Catal. A. 2007. 318: 155-159

Shell Oil Company. Olefin Disproportionation Catalyst and Process. USP 5114899. 1992a-5-19

Shell Oil Company. Olefin Disproportionation Catalyst and Process. USP 5098876. 1992b-5-24

Shell Oil Company. Olefin Disproportionation Catalyst and Process. USP 5210365. 1993a-5-11

Shell Oil Company. Olefin Disproportionation Catalyst and Process. USP 5254786. 1993b-10-19

Spamer A, Dube T I, Moodley D J, et al. Application of WO_3/SiO_2 catalyst in an industrial environmenta: Part II. Appl. Catal. A. 2003. 255: 133-142

van Schalkwyk C, Spamer A, Moodley D J, et al. Factors that could influence the activity of a WO_3/SiO_2 catalyst: Part III. Appl. Catal. A. 2003. 255: 143-152

Voorhies A. Carbon formation in catalytic cracking. Ind. Eng. Chem. 1945. 37(4): 318-322

Wang Y D, Chen Q L, Yang W M, et al. Effect of support nature on WO_3/SiO_2 structure and butene-1 metathesis. Appl. Catal. A. 2003. 250: 25-37

Wilson M E, Nuzzo R G and Whitesides G M. Stereochemistry of the degenerate metathesis of terminal alkenes—The nature of the chain-carrying metal-carbene complex. J. Am. Chem. Soc. March 29, 1978. 2270-2272

Zhao Q, Chen S L, Gao J, et al. Effect of tungsten oxide loading on metathesis activity of ethene and 2-butene over WO_3/SiO_2 catalysts. Transition Met. Chem. 2009. 34: 621-627

(Edited by Zhu Xiuqin)